Investigation of the substituting effect of Se on the physical properties and performances of $CdSe_xTe_{1-x}$ and $ZnSe_xTe_{1-x}$ materials for semiconductor radiation detectors

R. Malki, A. Tebboune*, L. Ghalouci, A. Saim, and A.H. Belbachir

Laboratoire d'Analyse et Applications des Rayonnements (LAAR), Département de Génie Physique, Faculté de Physique, Université des Sciences et de la Technologie d'Oran Mohamed Boudiaf, USTO-MB, BP1505 El Mnaouer, Oran 31000, Algeria.

**e-mail: tebbouneabdelghani@yahoo.fr*

Received 7 December 2020; accepted 23 February 2021

In this work, structural and electronic properties of $CdSe_xTe_{1-x}$ and $ZnSe_xTe_{1-x}$ semiconductor detectors at various concentrations $x = 0, 0.25, 0.5, 0.75$ and 1 of Selenium (Se) have been determined using the full potential-linearized augmented plane wave (FP-LAPW) based on the density functional theory (DFT). The lattice parameters results show good agreement when compared with reports. Band structure calculations indicate direct gap transitions and also yield the energy gap values, with good agreement with reports. Geant4 simulations have yielded the absolute and full-energy peak detection efficiencies and energy resolution at $1.5'' \times 1.5''$ of these alloys as semiconductor detectors in the 511-1332 keV gamma-ray energy range. Results are in a good agreement with the available theoretical and experimental data.

Keywords: $CdSe_xTe_{1-x}$; $ZnSe_xTe_{1-x}$; FP-LAPW; DFT; Geant4; Full-energy peak efficiency; absolute efficiency.

PACS: 02.70.Uu; 07.85.Nc ; 29.40.-n; 31.10.+z; 31.15.E-; 32.70.Fw; 73.20.At

DOI: https://doi.org/10.31349/RevMexFis.67.041002

1. Introduction

The last few years have witnessed an incredibly great interest in wide band gap IIB-VIA semiconductor materials due to their high performance in optoelectronic devices such as light emitting diodes [1], laser diodes [2], photovoltaic cells [3], solar cells [4], infrared optics and biological imaging [5]. Among this family, ternary alloys such as $CdSe_xTe_{1-x}$ and $ZnSe_xTe_{1-x}$ owned unique physical and chemical properties which might not be available in their parent binary systems (CdTe, CdSe, ZnTe and ZnSe) [6]. For this reason, the ternary systems can be performed to tune several physical properties of semiconductors and hence insight into the use in various potential applications are given. Recently, $CdSe_xTe_{1-x}$ ternary alloys have many applications in thin film photovoltaic due to their band gap bowing [7]. Experiments have identified nanostructured solar cells based on $CdSe_xTe_{1-x}$ as highly effective efficient and cost-efficient alternatives to conventional photovoltaic cells based on silicon [8]; $CdSe_xTe_{1-x}$ nanocrystals present themserlves as efficient and promising alloys for the manufacture of solar cells at low cost and in large area [9]. Furthermore, in the case of $ZnSe_xTe_{1-x}$ ternary alloys, experimental studies have employed them, *e.g*, for the synthesis of nanowires and in the study of the composition and size dependence of their optical gaps [10]. Also, they were studied for measurements of their reflectivity (RF), photoconductivity (PC), photoluminescence (PL) where it was found that the band gap-energy presents a minimum value at a selected composition ($x = 0.65$) [11], their bandgap bowing [6], the optical characterization, and application-oriented studies of $ZnSe_xTe_{1-x}$ ternary alloy nanowires [12]. Besides, some theoretical searchers have been carried out in the framework of the DFT approach to determine different physical properties of both $CdSe_xTe_{1-x}$ [13-15] and $ZnSe_xTe_{1-x}$ [16, 17] ternary alloys. On the other hand, semiconductor radiation detectors are widely used in several areas including nuclear physics, X-ray and gamma ray astronomy, and nuclear medicine. Most recently, an extensive effort has been invested to develop a range of semiconductor gamma ray detectors with wide band gap and high atomic number. Among them, cadmium telluride (CdTe) and cadmium zinc telluride (CdZnTe) are the most promising materials for radiation detectors showing high detection efficiency, promising energy resolution and good room temperature performance [18,19]. To the best of our knowledge, the performance of II-VI semiconductors based on selenium binary and ternary alloys have been reported for the first time using Monte Carlo simulations.

Our main contribution in the field of research is the prediction of new materials for the detection of radiation. For this reason, in the present work, we have performed an ab initio study based on the density functional theory (DFT) to investigate the physical properties namely structural and electronic properties of $CdSe_xTe_{1-x}$ and $ZnSe_xTe_{1-x}$ ternary alloys in the zinc blende structure. The alloy composition has been varied over the whole range of Se content starting from $x = 0$ (CdTe/ ZnTe) up to $x = 1$ (CdSe/ ZnSe). On the other side, we used the Geant4 toolkit for modelling and simula-

tion of radiation detection. This work will contribute to the development of the database to synthesize new materials for detection of radiation and can be miniaturized.

The paper is organized as follows: In Sec. 2, a brief description of the methods employed where details of the calculations are given. In Sec. 3, the results of structural and electronic properties of the ternaries in question are presented and analysed, then the results of the Geant4 simulations are presented. Finally, a conclusion is drawn in the last section.

2. Materials and methods

In this paper, the calculations were performed using the full-potential linearized augmented plane wave (FP-LAPW) approach [20] based on the density functional theory (DFT) [21] as implemented in the `wien2k` software package [22,23]. For the structural properties, the exchange-correlation (XC) effects were dealt with the Perdew-Burke-Ernzerhof generalized gradient approximation (PBE-GGA) [24] while for the electronic properties, the XC potentials were treated using the modified Becke-Johnson (mBJ) scheme [25,26].

In the FP-LAPW methodology, the unit cell was decomposed into two regions: Spheres centered at the nuclear sites and the interstitial zone between non-overlapping areas. Inside of the atomic spheres, the wave functions are expanded by spherical harmonics with a maximum quantum l number of $I_{\max} = 10$. Meanwhile, in the remaining space of the unit cell, the function is expanded in the form of plane waves with a cut-off parameter of $K_{\max} = 8/R_{MT}$, where R_{MT} is the smallest muffin-tin radius and the $K_{\max}$ is the magnitude of the largest vector in the plane wave expansion. To ensure convergence in the integrals over the first Brillouin zone, the calculations were performed using a mesh of 1000 K-points in the full Brillouin zone. Both of the plane wave cut-off parameter and the number of k-points have been varied in a way to ensure an accurate convergence of the total energy, which was achieved via self-consistent field (SCF) calculations with an energy threshold value of 10^{-4} Ry. The ternary alloys $CdSe_xTe_{1-x}$ and $ZnSe_xTe_{1-x}$ are formed from the four binary compounds CdSe, CdTe, ZnSe, and ZnTe. Hence, the eight-atom $1 \times 1 \times 1$ cubic zinc blende unit cell of the said binary compounds is designed by using their experimental lattice parameters in the introductory phase. The eight-atom cubic investigated ternary alloys $CdSe_xTe_{1-x}$ and $ZnSe_xTe_{1-x}$ with $x = 0.25$, 0.50 and 0.75 are designed by successive substitution of Te atom(s) with Se atom(s) in the $1 \times 1 \times 1$ unit cell of ZnTe and CdTe, respectively. Figure 1 illustrates the structures of the $CdSe_xTe_{1-x}$ ternary alloys as an example at all the selected compositions x. For $ZnSe_xTe_{1-x}$ ternary alloys, the Zn atoms replace the Cd atoms, because the structures are similar.

Additionally, we have carried out a Geant4-based Monte Carlo simulation in order to estimate the detection efficiency for all investigated semiconductors detectors at different photon energies. Geant4 is a robust software to describe the interactions of ionizing radiation with matter in high energy experiments, based on object oriented methodology and C++ language [27,28]. Its areas of applications include high energy, nuclear and accelerator physics as well as space engineering, medical sciences and radiation protection [29]. A main class controls the initialization of the geometry, physics and primary particle generation, which is the G4RunManager. The user has full freedom to develop its own simulation program. The geometry of our proposed model was coded in the mandatory class (Detector Construction) where we first designed the entire hall, which is referred in Geant4 as a world. Then, we modelled the geometry, materials and the sensitive region of the detector. A solid cylindrical detector of radius 1.5 inch and length 1.5 inch kept at a fix distance from the source [30] was simulated. The materials studied are $CdSe_xTe_{1-x}$ and $ZnSe_xTe_{1-x}$ alloys at various concentration $x = 0, 0.25, 0.5, 0.75$ and 1 which are used as semiconductor crystals. The type of emitted particle and its energy is set in the Primary Generator Action command of Particle Gun class. The primary particle defined was a gamma, emitting photons of energies in the energy range 511-1332 keV from 22-Na, 60-Co and 137-Cs radioactive sources and were placed at different distances (1, 2, 3, 5 and 10 cm) [30] from the face of detector. The simulation has been performed for each source. The physics processes are defined in the mandatory class (Physics List).

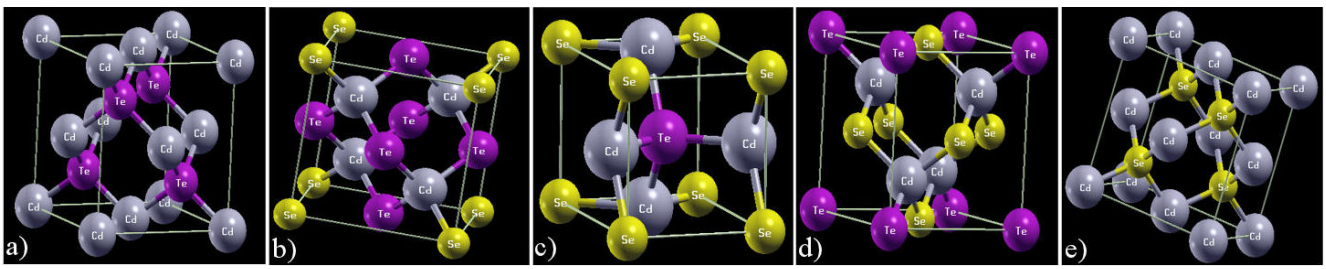

FIGURE 1. A geometry of the studied ternary alloys $CdSe_xTe_{1-x}$: a): $x = 0$, b): $x = 0.25$, c) $x = 0.50$, d) $x = 0.75$, e) $x = 1$). The atoms of Cd are with silver color, the Se atoms are with gold color while the Te atoms are with magenta color.

TABLE I. Atomic positions for $CdSe_xTe_{1-x}$ alloys.

x	Atom	Positions
0.25	Cd	(0.25, 0.75, 0.75), (0.75, 0.25, 0.75), (0.75, 0.75, 0.25), (0.25, 0.25, 0.25)
	Se	(0, 0, 0)
	Te	(0, 0.5, 0.5), (0.5, 0, 0.5), (0.5, 0.5, 0)
0.50	Cd	(0.25, 0.25, 0.25), (0.75, 0.75, 0.25), (0.75, 0.25, 0.75), (0.25, 0.75, 0.75)
	Se	(0.5, 0, 0.5), (0, 0.5, 0.5)
	Te	(0,0,0), (0.5, 0.5, 0)
0.75	Cd	(0.25, 0.25, 0.25), (0.75, 0.75, 0.25), (0.75, 0.25, 0.75), (0.25, 0.75, 0.75)
	Se	(0.5, 0.5, 0), (0, 0.5, 0.5), (0.5, 0, 0.5)
	Te	(0,0,0)

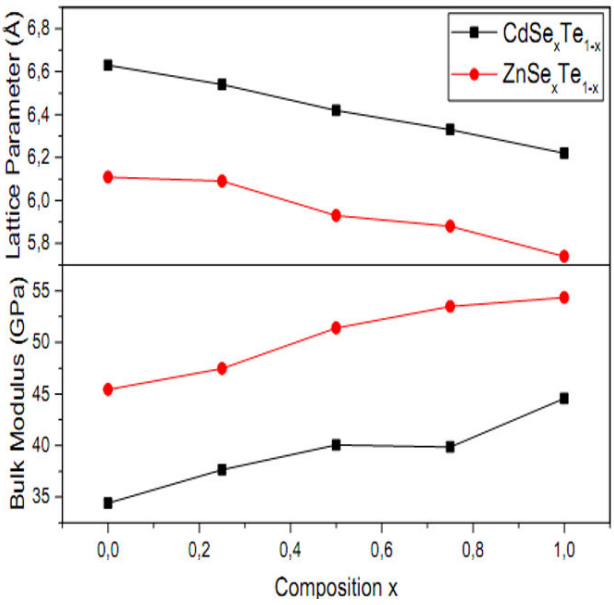

FIGURE 2. Composition dependence of calculated lattice constant and bulk modulus of $CdSe_xTe_{1-x}$ and $ZnSe_xTe_{1-x}$.

3. Results

3.1. Structural properties

The ternary alloys $CdSe_xTe_{1-x}$ and $ZnSe_xTe_{1-x}$ are bounded by four binary compounds of CdTe, CdSe, ZnTe and ZnSe. The investigated materials alloys were modelled in the zinc blende structure at various concentration $x = 0, 0.25, 0.5, 0.75$ and 1 with ordered structures using the construction of the eight-atoms supercell used by Agrawal *et al.* [31]. Several researchers have adopted this method to determine various properties of alloys [32-34]. As a prototype, the atomic positions of $CdSe_xTe_{1-x}$ are displayed in Table I. To determine the ground state properties such as the equilibrium lattice constant a_0 and the bulk modulus B_0 and the first-order derivative of bulk modulus (B'), the total energies were calculated for different volumes around the equilibrium cell volume V_0 and were adjusted to the Murnaghan equation of state [35]. The calculated structural parameters for the specimens at different compositions x along with previous experimental data and theoretical calculations reported in the literature are collected in Table II.

Our computed lattice constants for binary compounds showed best agreement with the experimental findings, though the computed B_0 is marginally underestimated. To the best of our knowledge, there are no available experimental structural data for $CdSe_xTe_{1-x}$ and $ZnSe_xTe_{1-x}$ ternary alloys for comparison. However, our computed results of a_0 and B_0 are compared with few earlier theoretical calculations in the literature, showing a good agreement, while the calculated B_0 values are marginally over estimated with respect to corresponding earlier theoretical data.

The variations of our obtained lattice constants a_0 and bulk modulus B_0 for $CdSe_xTe_{1-x}$ and $ZnSe_xTe_{1-x}$ ternary alloys against fraction x are traced out in Fig. 2. We can note that the lattice parameter a_0 decreases with increasing anionic selenium concentration x monotonically and almost linearly. In fact, it should be related to the substitution of tellurium atoms with greater radius by selenium atoms with smaller radius. A small deviation from Vegard's law [36] is found for both $CdSe_xTe_{1-x}$ and $ZnSe_xTe_{1-x}$ alloys with upward weak bowing parameters of -0.01 Å and -0.14 Å respectively, obtained by fitting the calculated values with a polynomial function.

On the other hand, for the bulk modulus, a visible deviation from Vegard's law from the linear concentration dependence was observed exhibiting downward boing to the order 0.66 GPa and 4.82 GPa for $CdSe_xTe_{1-x}$ and $ZnSe_xTe_{1-x}$ respectively. This deviation is mainly owing to the mismatch of the bulk modulus of the corresponding terminal binary compounds.

3.2. Electronic properties

The investigation of the electronic properties of semiconductors is significant to study their accuracy for the fabrication of a variety of technological devices. In the present work, in addition to GGA functional, TB_mBJ formalism is also utilized to investigate the electronic properties of the ternary alloys studied from the computed equilibrium lattice parameters.

3.2.1. Band structure

The calculations of the band structures of the specimens under each of $CdSe_xTe_{1-x}$ and $ZnSe_xTe_{1-x}$ systems were performed at the optimized lattice constants using the mBJ scheme. Therefore, the band structures of the five specimens under the $CdSe_xTe_{1-x}$ ($x = 0, 0.25, 0.50, 0.75, 1$) ternary alloys are represented in Fig. 3 (as a prototype). It is obvious that the valence band maximum (VBM) and conduction band

TABLE II. Calculated equilibrium lattice parameter a_0(Å) and bulk modulus B_0 (GPa) for the binary compounds CdSe, CdTe, ZnSe and ZnTe and their ternary alloys $CdSe_xTe_{1-x}$ and $ZnSe_xTe_{1-x}$.

Material	a (Å)	B (GPa)	Method	References
This work			Generalized gradient approximation of Perdew-Burke-Ernzerhof (GGA-PBE)	
CdTe	6.63	34.42		
$CdSe_{0.25}Te_{0.75}$	6.54	38.42		
$CdSe_{0.50}$ $Te_{0.50}$	6.42	39.85		
$CdSe_{0.75}Te_{0.25}$	6.33	40.06		
CdSe	6.22	44.58		
Other calculations				
CdTe	6.48	44.50	Experimental	[40]
	6.62	46.60	GGA-PBE	[41]
	6.64	36.24	GGA-PBE	[14]
	6.52	40.13	GGA-PBE	[14]
	6.53	38.86	GGA-PBE	[15]
	6.41	42.20	GGA-PBE	[14]
	6.43	40.86	GGA-PBE	[15]
	6.32	43.07	GGA-PBE	[14]
	6.33	43.54	GGA-PBE	[15]
	6.05	53.00	Experimental	[40]
	6.21	45.60	GGA-PBE	[41]
	6.20	44.86	GGA-PBE	[42]
This work			Generalized gradient approximation of Perdew-Burke-Ernzerhof (GGA-PBE)	
ZnTe	6.11	48.42		
$ZnSe_{0.25}Te_{0.75}$	6.09	47.48		
$ZnSe_{0.50}Te_{0.50}$	5.93	51.40		
$ZnSe_{0.75}Te_{0.25}$	5.88	53.50		
ZnSe	5.74	62.42		
Other calculations				
ZnTe	6.10	48.39	Experimental	[40]
	6.10	46.60	GGA-PBE	[33]
	6.07	36.24	GGA-PBE	[43]
	6.52	40.13	GGA-PBE	[17]
	6.53	38.86	GGA-PBE	[33]
	6.41	42.20	GGA-PBE	[33]
	6.43	40.86	GGA-PBE	[17]
	6.32	43.07	GGA-PBE	[33]
	6.33	43.54	GGA-PBE	[17]
	6.05	53.00	Experimental	[40]
	6.10	45.60	GGA-PBE	[43]
	6.07	44.86	GGA-PBE	[32]

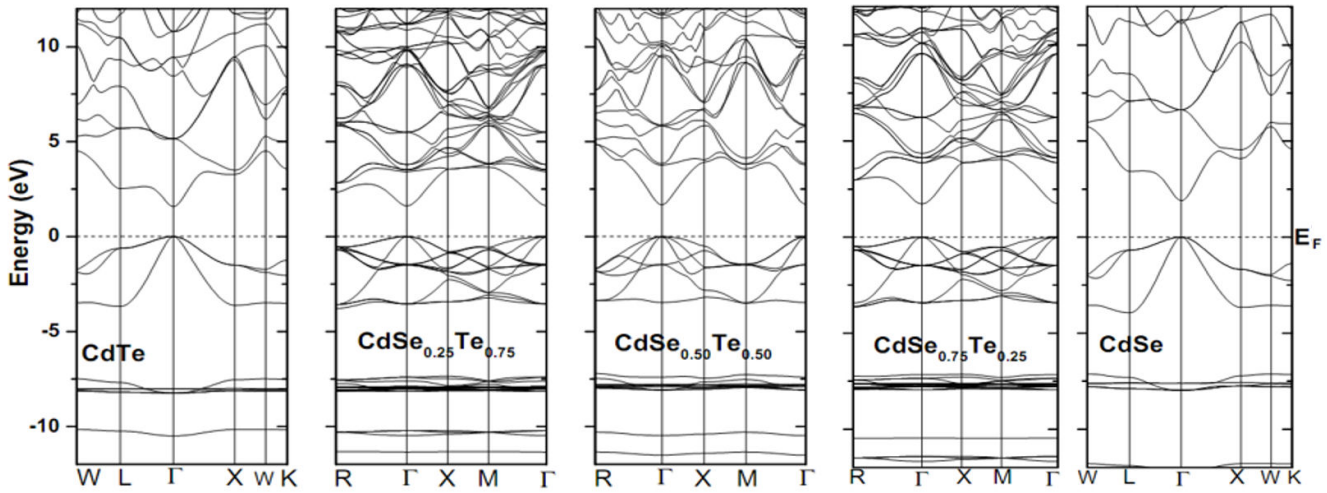

FIGURE 3. Band structure for $CdSe_xTe_{1-x}$. ($x = 0, 0.25, 0.50, 0.75, 1$).

minimum (CBM) lie at the Γ-symmetry point resulting in the direct ($\Gamma - \Gamma$) bandgap in the zinc blende phase. It is also observed that the qualitative features of band structures of each of the said ternary alloys are almost same at any specific (Se) concentration x.

3.2.2. *Bandgap*

The bandgap values for each of the said alloys calculated using the GGA-PBE and mBJ schemes are presented in Table III as well as some experimental and earlier theoretical data. It is shown that our predicted band gap values for the binary compounds CdSe, CdTe, ZnSe and ZnTe using the mBJ functional reveal good agreement with the corresponding experimental outcomes. In contrast, the results performed within the GGA-PBE approximation are on the hole underestimated. No experimental findings for both $CdSe_xTe_{1-x}$ and $ZnSe_xTe_{1-x}$ ternary alloys in the literature for comparison. Then, the calculated band gap energies for each ternary system agree well with respect to the corresponding earlier theoretical data for $CdSe_xTe_{1-x}$ and $ZnSe_xTe_{1-x}$.

Figure 4 illustrates the variation of the obtained band gap energies as a function of the composition x in the zinc blende phase with the equilibrium lattice constants. It can be seen that the calculated band gap increases nonlinearly with the increasing anionic (Se) concentration with each GGA-PBE and mBJ approaches, respectively for all materials of interest providing an upward bowing, where -0.18 eV and -0.22 eV bowing is observed for $CdSe_xTe_{1-x}$ and $ZnSe_xTe_{1-x}$ respectively.

TABLE III. The minimum band gap energy of $CdSe_xTe_{1-x}$ and $ZnSe_xTe_{1-x}$ ternary alloys calculated using the GGA-PBE and mBJ functionals at equilibrium volume (all values are in eV).

	Present		Exp.	Others
Material	GGA-PBE	mBJ		
$CdSe_xTe_{1-x}$				
0	0.60	1.62	1.60 [40]	0.76 [14], 1.60 [33]
0.25	0.79	1.75	–	0.83 [14], 1.81 [33]
0.50	0.80	1.80	–	0.89 [14], 1.88 [33]
0.75	0.85	1.87	–	0.95 [14], 1.90 [33]
1	0.95	1.91	1.90 [40]	1.90 [33]
$ZnSe_xTe_{1-x}$				
0	0.98	2.40	2.39 [40]	0.58 [17], 2.40 [33]
0.25	1.16	2.42	–	0.86 [17], 2.42 [33]
0.50	1.31	2.58	–	0.83 [17], 2.50 [33]
0.75	1.44	2.61	–	0.90 [17], 2.63 [33]
1	1.53	2.83	2.82 [40]	1.10 [17], 2.86 [33]

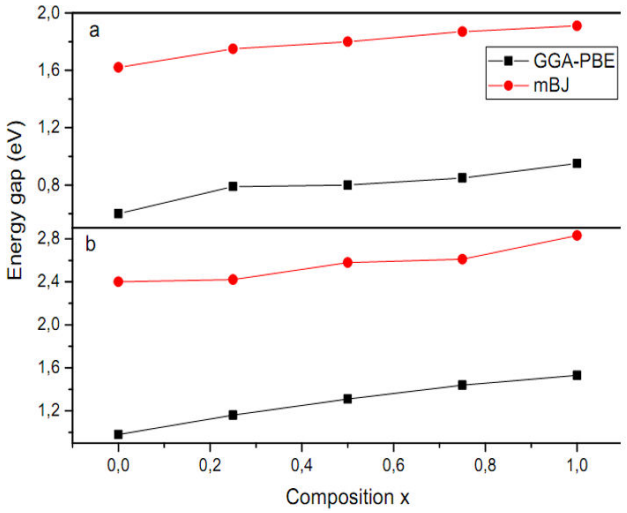

FIGURE 4. Composition dependence of the calculated band gap using GGA-PBE and mBJ for a) $CdSe_xTe_{1-x}$ and b) $ZnSe_xTe_{1-x}$ alloys.

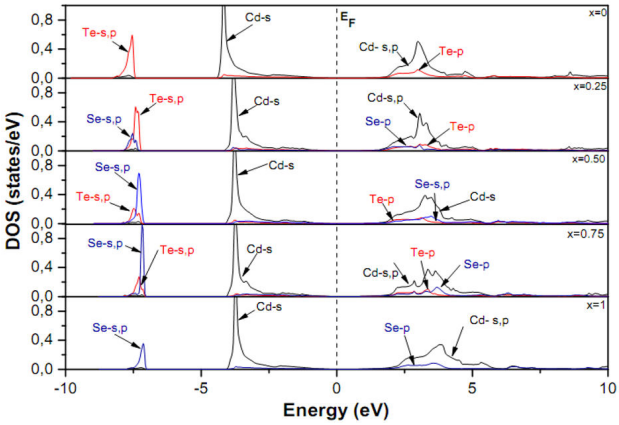

FIGURE 5. Density of states for $CdSe_xTe_{1-x}$. ($x = 0, 0.25, 0.50, 0.75, 1$).

3.2.3. Density of states

Studies on the density of states of any material drives us to a profound insight into the character of their band states and the determination of the electronic properties. In the present section, we have computed the total and partial densities of states for each of CdSe, CdTe, ZnSe, ZnTe and their ternary alloys, but only the PDOS of $CdSe_xTe_{1-x}$ system are represented for the whole range of the concentration x (as an example) in Fig. 4 because the electronic state contribution of the other alloy is similar.

It can be seen from Fig. 5 that the TDOS comprises three distinguished regions: the lower valence band (LVB), upper valence band (UVB) and the conduction band (CB), respectively. The Fermi energy level E_F in all the PDOS plots is set to origin and shown by dotted line. Besides, one can observe that the different regions of the valence and conduction bands are dominated by various orbitals of the Cd, Se and Te atoms. Then, the contribution of the two-chalcogenide orbitals results from the combined contribution of Se and Te atoms. Additionally, the contribution from different orbitals of Selenium atoms progressively increases while those of Tellurium atoms gradually decrease with increasing Selenium concentration. The lower conduction band has a mixed character of p states of Cd, Se and Te.

3.3. Geant4 simulation

The simplified simulated detector is considered as cylinder with external dimensions of $1.5''$ in radius and $1.5''$ in length. The simulations are carried out for a very large number of events (the order of 10^6) for all the chosen energies and the detectors. The point source was defined to produce isotropic emission and was positioned first at a fixed distance from the face of the detector for all the said materials, and then we have varied the distance taking all the possible physics processes into account. The energy deposited in the detector has been calculated and the output files in ASCII format were

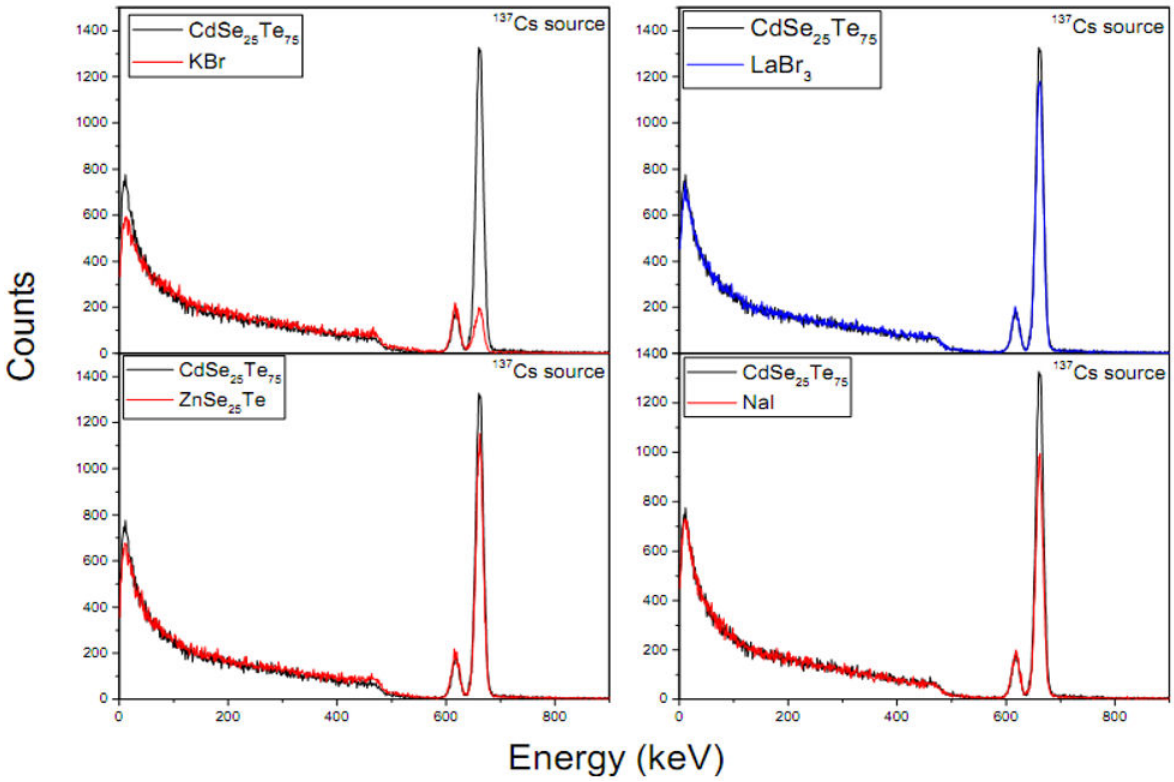

FIGURE 6. The energy spectrum recorded for (1.5 inch. $\times$ 1.5 inch.) cylinders of $CdSe_xTe_{1-x}$ and $ZnSe_xTe_{1-x}$ ($x = 25$) semiconductors and $LaBr_3$ scintillator from a 137-Cs source.

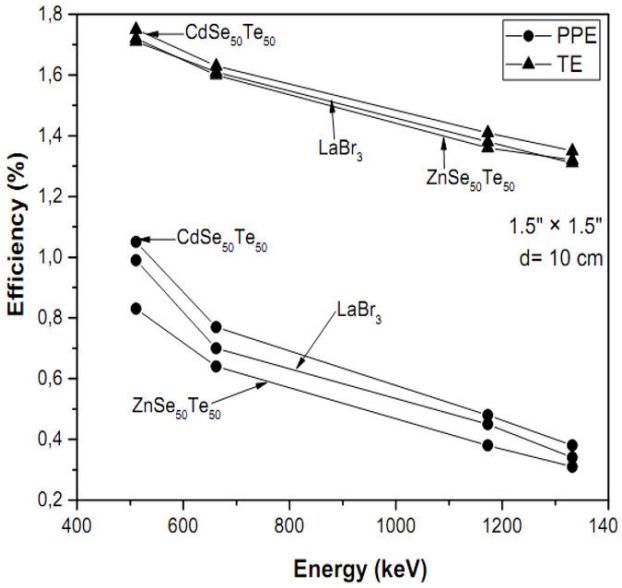

FIGURE 7. The energy dependent total and photopeak efficiencies for (1.5 inch. × 1.5 inch.) cylinders of $CdSe_xTe_{1-x}$ and $ZnSe_xTe_{1-x}$ semiconductors and $LaBr_3$ scintillator.

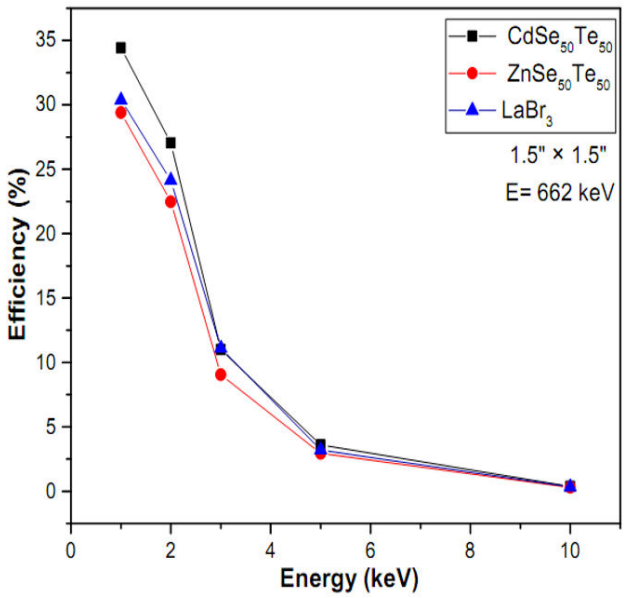

FIGURE 8. Variation of photopeak efficiency of $CdSe_xTe_{1-x}$, $ZnSe_xTe_{1-x}$ and $LaBr_3$ detector as a function of distance.

generated for each simulation. The performances have been compared with performances of the $LaBr_3$ scintillator detector of equivalent volume.

The properties such as energy resolution, absolute and photo peak detection efficiencies of the said materials have been measured for 5 different gamma ray energies. Then, the distance from the source to the detector face was varied to observe the effects on the semiconductor detector efficiency.

The extraction of efficiencies for sources emitting monoenergetic gamma-rays can be obtained from the total and the photo-peak areas. The absolute and the full-energy peak detection efficiencies can be defined as [37,38] :

$$\varepsilon_{\text{abs}} = \frac{\text{total number.of gammas detected}}{\text{total number.of gammas emmited by source}}, \quad (1)$$

$$\varepsilon_{\text{peak}} = \frac{\text{number.of gammas detected under photopeak}}{\text{number.of gammas emmited by source}}. \quad (2)$$

The detection efficiencies were obtained using Eqs. (1) and (2) for each gamma ray energy emitted by the 22Na, 60Co, and 137Cs radioactive isotopes. We have reported in Fig. 6 the simulated energy spectrum from 137-Cs recorded with $CdSe_{25}$ Te_{75}, $ZnSe_{25}$ Te_{75}, $LaBr_3$, NaI and KBr materials for comparison.

Figure 6 displays the variation of the energy dependent efficiencies from 551 keV to 1332 keV for $CdSe_xTe_{1-x}$, $ZnSe_xTe_{1-x}$ (for $x = 0.50$) and $LaBr_3$ of equivalent volume. The point source was kept at 10 cm from the face of each detector. It was found that the variation of the absolute efficiency of $CdSe_{50}$ Te_{50} seems to be rather better than $ZnSe_{50}$ Te_{50} and $LaBr_3$. From 511 keV to 662 keV and beyond 1200 keV, $ZnSe_{50}$ Te_{50} shows marginally better efficiency than $LaBr_3$, maintaining by the way very slight differences among them. The photo peak efficiency of $CdSe_{50}$ Te_{50} remained higher than $ZnSe_{50}$ Te_{50} and $LaBr_3$. It can also be shown from this figure, the efficiencies decrease when the energy increases. The results show that CdSeTe is better than all the other studied materials. Nevertheless, both CdSeTe ternary alloy and $LaBr_3$ seem to be almost similar, with slight difference. Good agreement is found in comparison with other results [39]. Figure 8 shows the variation of the detection efficiency versus the distance from the detector face for 5 different distances. It was found that the full energy peak efficiency of the detector varies when the distance from the source to the detector face was changed. It can be seen

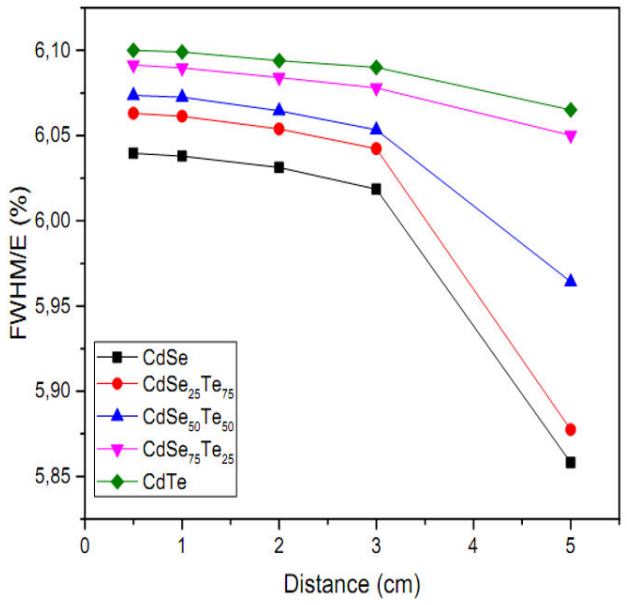

FIGURE 9. Energy resolution of $CdSe_xTe_{1-x}$ detectors obtained from 60Co versus distance.

also that the detection efficiency has decreased with the increasing distance from detector face.

3.3.1. The energy resolution

The energy resolution of a detector system is obtained from the peak full width at one-half of the maximum height (FWHM) of a single peak using the following equation:

$$R = \frac{FWHM}{E_0} \times 100, \tag{3}$$

where R is the energy resolution and E_0 is the related energy. The energy resolution of the investigated detectors is displayed in Fig. 9 as a function distance. It can be seen from this figure that the energy resolution of all the said materials decreased with the increasing distance.

4. Conclusion

In the current paper, the structural and electronic properties of $CdSe_xTe_{1-x}$ and $ZnSe_xTe_{1-x}$ ternary alloys at various concentration ($x = 0, 0.25, 0.50, 0.75, 1$) were studied using the full potential linearized augmented plane wave method. The computed equilibrium lattice constants and bulk moduli were in good agreement with earlier experimental and theoretical outcomes. We have found that the variation of the structural parameters and the band gap does not obey Vegard's law and depends non-linearly on the selenium concentration. Besides, the electronic band structure calculations demonstrate that the incorporation of Se in CdTe and ZnTe increases the band gap. On another side, the full-energy peak and absolute efficiencies of II-VI ternary alloy gamma-ray detectors were determined by Geant4 simulations. The variation of detection efficiency with the gamma ray energy and detection distance was also investigated. The results show that the detection efficiencies of $CdSe_xTe_{1-x}$ ternary alloy are higher than the corresponding $ZnSe_xTe_{1-x}$ $LaBr_3$ and NaI efficiencies. It was also found from this work that the detection efficiency depends on gamma ray energy and source distance to the detector. Our semiconductor materials are potential candidates for radiation detectors. We hope that our results serve as a reference for future theoretical and experimental researches.

1. S. Coe, W. K. Woo, M. Bawendi, V. Bulovic, Electroluminescence from single monolayers of nanocrystals in molecular organic devices, *Nature*. **420** (2002) 800, https://doi.org/10.1038/nature01217
2. S. Kasap, P. Capper, Wide-Bandgap II-VI Semiconductors: Growth and Properties. Springer Handbook of Electronic and Photonic Materials edited by S. Kasap and P. Capper (Springer, Cham, 2017), https://doi.org/10.1007/978-3-319-48933-9_16.
3. B. O'regan, M. Graetzel, A low-cost, high-efficiency solar cell based on dye-sensitized colloidal TiO_2 films, *Nature.* **353** (1991) 737, https://doi.org/10.1038/353737a0
4. W. U. Huynh, J. J. Dittmer, A. P. Alivisatos, Hybrid Nanorod-Polymer Solar Cell, *Science.* **295** (2002) 2425, https://doi.org/10.1126/science.1069156.
5. J. K. Jaiswal, H. Mattoussi, J. M. Mauro, S. M. Simon, Long-term multiple color imaging of live cells using quantum dot bioconjugates, *Nat Biotechnol*. **21** (2003) 47, https://doi.org/10.1038/nbt767.
6. F. Xu, B. Xue, F. Wang, A. Dong, Ternary alloyed $ZnSe_xTe_{1-x}$ nanowires: Solution-phase synthesis and band gap bowing, *Chem. Mater*. **27** (2015) 1140, https://doi.org/10.1021/acs.chemmater.5b00070
7. M. Lingg, S. Buecheler, and A. N. Tiwari, Review of $CdTe_{1-x}Se_x$. Thin Films in Solar Cell Applications, *Coatings* **9** (2019) 520, https://doi.org/10.3390/coatings9080520.
8. B. I. MacDonald *et al.*, Layer-by-layer assembly of sintered $CdSe_xTe_{1-x}$ nanocrystal solar cells, *ACS Nano*. **6** (2012) 5995, https://doi.org/10.1021/nn3009189.
9. S. Wen *et al.*, Rationally controlled synthesis of $CdSe_xTe_{1-x}$ alloy nanocrystals and their application in efficient graded bandgap solar cells, *Nanomaterials*. **7** (2017) 380, https://doi.org/10.3390/nano7110380.
10. H. Asano, K. Arai, M. Kita, and T. Omata, Synthesis of colloidal Zn (Te, Se) alloy quantum dots, *Mater. Res. Exp.* **4** (2017) 106501, https://doi.org/10.1088/2053-1591/aa8b84.
11. M. J. S. P. Brasil, R. E. Nahory, F. S. Turco-Sandroff, H. L. Gilchrist, and R. J. Martin, Evolution of the band gap and the dominant radiative recombination center versus the composition for $ZnSe_{1-x}Te_x$ alloys grown by molecular beam epitaxy, *Appl. Phys. Lett*. **58** (1991) 2509, https://doi.org/10.1063/1.104859.
12. J. Lu, H. Liu, X. Zhang, C. H. Sow, One-dimensional nanostructures of II-VI ternary alloys: synthesis, optical properties, and applications, *Nanoscale* **10** (2018) 17456, https://doi.org/10.1039/C8NR05019H.
13. M. Shakil *et al.*, Theoretical calculations of structural, electronic, and elastic properties of $CdSe_{1-x}Te_x$: a first principles study, *Chin. Phys. B.* **25** (2016) 076104, https://doi.org/10.1088/1674-1056/25/7/076104.
14. A.H. Reshak, I. V. Kityk, R. Khenata, S. Auluck, Efect of increasing tellurium content on the electronic and optical properties of cadmium selenide telluride alloys $CdSe_{1-x}$Tex: an ab initio study, *J. Alloys Compd*. **509** (2011) 6737, https://doi.org/10.1016/j.jallcom.2011.03.029.
15. S. Ouendadji, S. Ghemid, N. Bouarissa, H. Meradji, and F. El Haj Hassan. Ab initio study of structural, electronic, phase diagram, and optical properties of $CdSe_xTe_{1-x}$ semiconducting alloys, *J. Mater. Sci.* **46** (2011) 3855, https://doi.org/10.1007/s10853-011-5306-1.

16. Y. Zhu *et al.*, Structural, elastic, and thermodynamic properties of $ZnSe_xTe_{1-x}$: a first-principles study, *Comput. Mater. Sci*. **50** (2011) 2745, https://doi.org/10.1016/j.commatsci.2011.03.037.

17. F. El Haj Hassan, B. Amrani, F. Bahsoun, Ab initio investigations of zinc chalcogenides semiconductor alloys, *Phys. B.* **391** (2007) 363, https://doi.org/10.1016/j.physb.2006.10.020.

18. S. Del Sordo *et al*., Progress in the Development of CdTe and CdZnTe Semiconductor Radiation Detectors for Astrophysical and Medical Applications, *Sensors*. **9** (2009) 3491, https://doi.org/10.3390/s90503491.

19. C. G. Wahl *et al*., The Polaris-H imaging spectrometer, *Nucl. Instrum. Methods A*. **784** (2015) 377, https://doi.org/10.1016/j.nima.2014.12.110.

20. O. Krogh Andersen, Linear methods in band theory, *Phys. Rev. B.* **12** (1975) 3060, https://doi.org/10.1103/PhysRevB.12.3060.

21. W. Kohn and L. J. Sham, Self-Consistent Equations Including Exchange and Correlation Effects, *Phys. Rev*. **140** (1965) A1133, https://doi.org/10.1103/PhysRev.140.A1133

22. K. Schwarz, P. Blaha, and G. K. H. Madsen, Electronic structure calculations of solids using the WIEN2k package for material sciences, *Comput. Phys. Commun.* **147** (2002) 71, https://doi.org/10.1016/S0010-4655(02)00206-0

23. P. Blaha, K. Schwarz, K. Madsen, D. Kvasnicka, J. Luitz, FP-LAPW+lo program for calculating crystal properties, Technische. WIEN2K, Austria, 2001.

24. J. P. Perdew, K. Burke, M. Ernzerhof, Generalized Gradient Approximation Made Simple, *Phys. Rev. Lett*. **77** (1996) 3865, https://doi.org/10.1103/PhysRevLett.77.3865.

25. A. D. Becke and E. R. Johnson, A simple effective potential for exchange, *J. Chem. Phys.* **124** (2006) 221101, https://doi.org/10.1063/1.2213970.

26. F. Tran and P. Blaha, Accurate Band Gaps of Semiconductors and Insulators with a Semilocal Exchange-Correlation Potential, *Phys. Rev. Lett*. **102** (2009) 226401, https://doi.org/10.1103/PhysRevLett.102.226401.

27. S. Agostinelli *et al.*, Geant4-a simulation toolkit, *Nucl. Instrum. Methods Phys. Res. A*. **506** (2003) 250, https://doi.org/10.1016/S0168-9002(03)01368-8.

28. J. Allison *et al.*, Geant4 developments and applications, *IEEE Trans. Nucl. Sci.* **53** (2006) 270, https://doi.org/10.1109/TNS.2006.869826.

29. J. Allison *et al.* Recent Developments in Geant4. *Nucl. Instrum. Meth. A.* **835** (2016) 186, https://doi.org/10.1016/j.nima.2016.06.125.

30. I. Akkurt, K. Gunoglu and S. S. Arda, Detection Efficiency of NaI (Tl) Detector in 511-1332 keV Energy Range, *Sci. Technol. Nucl. Install*. **2014** (2014) 186798, https://doi.org/10.1016/j.nima.2016.06.125.

31. B. K. Agrawal, S. Agrawal, P. S. Yadav, S. Kumar, Ab initio calculation of electronic properties of $Ga_{1-x}AL_xN$ alloys, *J. Phys.: Condens. Matter*. **9** (1997) 1763, https://doi.org/10.1088/0953-8984/9/8/008.

32. S. Bendiaf *et al*., First-principle calculations of the structural, electronic, thermodynamic and thermal properties of ZnS_xSe_{1-x} ternary alloys, *Bull Mater Sci*. **38** (2015) 365, https://doi.org/10.1007/s12034-015-0877-0.

33. S. Chanda *et al.*, Calculations of the structural and optoelectronic properties of cubic $Cd_xZn_{1-x}SeyTe_{1-y}$ semiconductor quaternary alloys using DFT-based FP-LAPW approach, *J. Comput. Electron*. **19** (2020) 1, https://doi.org/10.1007/s10825-019-01409-0.

34. M. Tinoco, L. Maduro and S. Conesa-Boj, Metallic edge states in zig-zag vertically-oriented MoS_2 nanowalls, *Sci. Rep*. **9** (2019) 15602, https://doi.org/10.1038/s41598-019-52119-3.

35. F. D. Murnaghan, The compressibility of media under extreme pressures, *Proc. Natl. Acad. Sci. U.S.A.* **30** (1944) 244, https://doi.org/10.1073/pnas.30.9.244.

36. L. Vegard, The constitution of the mixed crystals and the space Occupied of the atom, *Z. Phys*. **5** (1921) 17, https://doi.org/10.1007/BF01349680.

37. G. F. Knoll, *Radiation Detection and Measurement*, 4th ed. (Wiley, New York, 2000), pp. 720-722.

38. J. Singh, A. Koblov, Excitonic processes and their contribution to nonproportionality observed in the light yield of inorganic scintillators, *Eur. Phys. J. B.* **86** (2013) 33, https://doi.org/10.1140/epjb/e2012-30693-9.

39. N. Belameiri *et al.*, Comparative study on performance and physical properties of CsI, NaI, RbI, and KBr materials, *Can. J. Phys.* **94** (2016) 1378, https://doi.org/10.1139/cjp-2016-0372.

40. O. Medelung, *Landolt Bornstein Numerical Data and Functional Relationship in Science and Technology*, (Springer, Berlin, 1982), pp. 17.

41. L. Guo , S. Zhang, W. Feng, G. Hu, W. Li, A first-principles study on the structural, elastic, electronic, optical, lattice dynamical, and thermodynamic properties of zinc-blende CdX (X = S,Se, and Te), *J. Alloys Compd*. **579** (2013) 583https://doi.org/10.1016/j.jallcom.2013.07.096.

42. S. Ouendadji, S. Ghemid, H., Meradji, F. El Haj Hassan, Theoretical study of structural, electronic, and thermal properties of CdS, CdSe and CdTe compounds, *Comput. Mater. Sci*. **50** (2011) 1460, https://doi.org/10.1016/j.commatsci.2010.11.035.

43. M. Bilal, M. Shafiq, I. Ahmad, I. Khan, First principle studies of structural, elastic, electronic and optical properties of Zn-chalcogenides under pressure, *J. Semicond*. **35** (2014) 072001, https://doi.org/10.1088/1674-4926/35/7/072001.